

Online IR Sensor-based Grasp Planner for the Pisa/IIT SoftHand

E. Luberto¹, G. Santaera¹, Y. Wu¹, M. Gabiccini^{1,2,3}, and A. Bicchi^{1,3}

Abstract—This paper presents an approach to refine grasps for soft robotic hands in the presence of uncertainty. Once a pre-planned grasp, e.g. from a database, has been selected for execution to an object detected in a scene, an infrared sensor-informed grasp planner is run that essentially reduces uncertainties related to object shape and its pose in the environment. The proposed method implements a grasp location optimization algorithm that allows to minimize the distances between hand fingertips and the object by continuously controlling the wrist pose and the amount of hand closing. Experimental studies with Kuka-lwr arm and Pisa/IIT Softhand illustrate the benefit of the developed technique and the improvement in the grasping performance with respect to the open-loop execution of grasps planned on the basis of prior visual cues only.

I. INTRODUCTION

The problem of autonomous robotic grasping has been in the focus of robotic research community for the past several decades [1], [2], [3]. Intelligent, proficient grasp planners have been developed that allow robotic hand to perform grasping tasks closely to humans. For ideal scenarios, where the object shape and location are perfectly known, and precise control of robotic hand can be achieved, pre-programmed autonomous grasping may be possible. To this end, most of the proposed planners [4], [5] rely on finding optimal fingertip placement on the object, while the surrounding environments are considered to be avoided as obstacles. However, these approaches are limited by their hand rigidity and fragility, and the manipulation strategies are very far from those a human would execute in real scenarios.

A real-world grasps are often associated to some uncertainties, the most typical ones being related to object recognition and localization. Usually, robots are equipped with vision sensors [6], [7], [8] to help reducing this uncertainty. However, a certain amount of uncertainty is usually unavoidable due to poor vision results, or incomplete view coverage of the sensor, etc. Other uncertainty may correspond to unexpected location of the object, where in this case, tactile/torque sensors are required to gain some additional information and to refine the object location from contacts [9], [10], [11]. Therefore, dexterous grasping of objects under uncertainty remains a difficult and unsolved problem in robotics.

¹Research Center “E. Piaggio”, Università di Pisa, Largo Lucio Lazzarino 1, 56122 Pisa, Italy

² Dipartimento di Ingegneria Civile e Industriale, Largo Lucio Lazzarino 1, 56122 Pisa, Italy

³ Department of Advanced Robotics, Istituto Italiano di Tecnologia, Via Morego 30, 16163 Genova, Italy

Corresponding author is: M. Gabiccini, Largo Lucio Lazzarino 1, 56122 Pisa, Italy. Tel. +39-050-221.80.77, Fax: +39-050-221.80.65, Email: m.gabiccini@ing.unipi.it.



Fig. 1. Pisa/IIT Softhand with IR sensors

To better tackle the above described types of uncertainty, researchers have proposed the use of underactuated and/or soft hands [12], [13]. The design is simpler, easier to control and allows object contact with hand parts other than the fingertips, as well as to explore the surrounding environment in order to achieve precise and stable grasp. The robotic hand studied in this paper is the Pisa/IIT Softhand [14], which has only one degree of actuation, and is continuously deformable in an infinity of possible shapes through interaction with objects and environment. Incipient grasp with this type of Softhand has been successfully achieved with a wide variety of everyday objects [15]. However, problems still remain when one or several above mentioned uncertainties occur during the execution of grasping tasks with novel objects.

The lack of exact knowledge of target object shape and location in the environment can be compensated by the use of sensor feedback. To further improve the quality and reliability of robotic grasping, different strategies have been proposed to enhance the sensing capabilities of robotic manipulators. Enhancement of long-range vision sensor is one of the solutions, such as in-hand object tracking, hand extraction for object reconstruction, etc. However in general, image acquisition and processing are quite slow for online reactive response. Another solution relies on tactile sensors, which have been employed in numerous tasks [16], [17], whereas they require premature contacts with the object and may cause significant object motion.

On the other hand, short-range infrared (IR) sensors are widely used in robotic applications thanks to their low-cost, fast response time and reduced sensitivity to the environment. In robotic grasping, IR sensors have been introduced during final grasp adjustments. In [18], the authors detect the

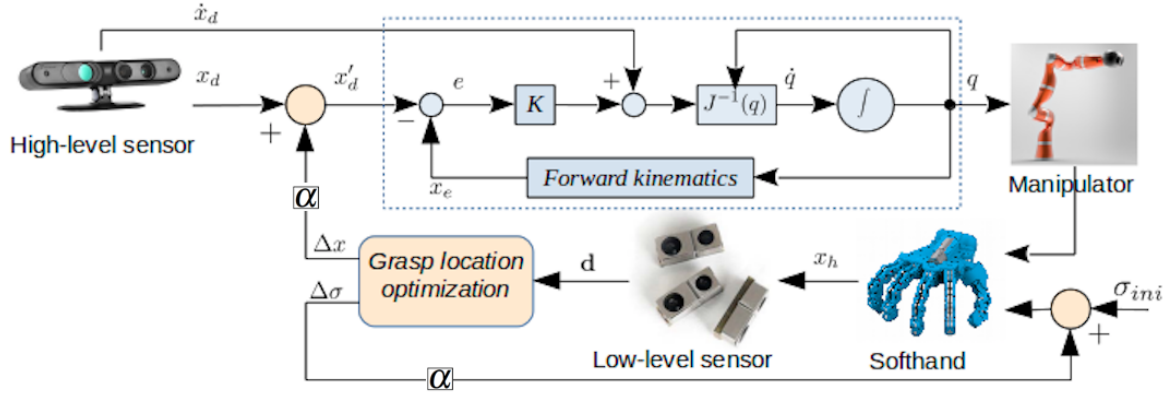


Fig. 2. Control scheme of sensor-based grasping

orientation of an object surface using the IR sensors that fit inside the fingers. In [19], a shared-control algorithm has been proposed based on long-range vision sensor and infrared sensors for teleoperation-based grasping. In [20], robust grasping has been achieved using an IR Net-structure proximity sensor for objects with unknown position and attitude. However, these approaches have been developed for robotic hands with sensible rigidity and high degrees of actuation (4-8). Limited number of work address the problem of grasping refinement for compliant hands based on IR sensor measurements, which looks very promising here.

In this work, an approach to grasp refinement for the Pisa/IIT Softhand under uncertainty using IR sensors is presented. Based on sensor measurement feedback, the proposed algorithm allows to center the Softhand fingers around the object and wrap the hand around it in a uniform manner. It is effective, high-speed, does not cause premature object contact nor needs re-grasping strategies. It allows the robotic hand to perform online adjustments before final grasping.

To address the above mentioned problems, the remainder of the paper is organized as follows. Section II presents the problem of grasping with our Softhand. Section III describes the IR sensor working principle and the measurements is provided. In Section IV, an algorithm of grasp location refinement of the Softhand is presented. Section V contains the experimental results obtained for IR sensor-based grasp of novel objects using Kuka-lwr and Pisa/IIT Softhand. Finally, Section VI summarizes the main results and contributions of this paper.

II. PROBLEM STATEMENT

Despite the fact that contemporary vision systems are able to reconstruct fairly good 3D object models, which allows to considerably reduce the related uncertainties, it requires enormous time and manpower to build a point cloud library for each novel object, yet still incomplete to guarantee a stable final grasp. To reduce the time of visual acquisition and processing, we propose to use only the prior visual cue of an object, which leads the robot to a so-called

pre-grasp location. In order to ensure a stable final grasp, infrared sensors are mounted on the hand fingertips to gain some additional information about the hand location with respect to the object.



Fig. 3. Types of uncertainty during grasping

For the considered compliant hand, due to the peculiarities of its embedded soft and adaptive synergy [14], its configuration and exact fingertip locations are usually unknown after a grasp is executed. Therefore, the target object is approached by the hand via controlling wrist pose and hand closing. In order to improve the quality of grasp, we proposed to minimize the distances between hand fingertips by continuously controlling the wrist pose and the amount of hand closing based on IR sensor measurements. As the hand is closed in an informed manner, the proposed method allows to reduce the chance of significantly perturbing the object during the execution of the final grasp.

The overall control scheme of the robotic arm and hand is depicted in Fig. 2. The proposed grasp location optimization algorithm provides the correction values of wrist pose and hand closing at each time step. This control strategy allows to effectively improve the quality of grasp under uncertainty, such as visual incompleteness and/or coverage, unexpected change of object location and motion, etc. (see Fig. 3).

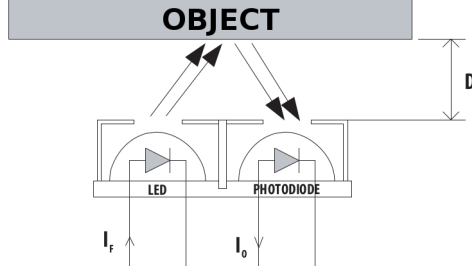


Fig. 4. Infrared sensor working principle

III. SENSOR MEASUREMENTS

To measure the distances between hand fingertips and target object, we proposed to use infrared sensor. Its advantages include small size, low-cost, mechanical robustness and the simplicity to be managed with a micro-controller. The sensor consists of only one emitter and one receiver (See Fig. 4). The intensity of the transmitted infrared wave decreases according to the well known exponential law

$$E = E_0 e^{-\alpha x}, \quad (1)$$

where E_0 is the intensity of the original wave, x depends on the wave direction, and the parameter α varies with the material and increases with the wave frequency.

When the transmitted wave meets an object it splits in two, a refracted wave that spreads onto the object and a reflected one that comes back and meets the receiver. The intensity of these two waves depends on the reflection coefficient of the object material and on the angle at which the transmitted wave hits the object. The relation between the transmitted, refracted and reflected wave can be obtained using the Snell's law

$$k_1 \sin \theta_1 = k_2 \sin \theta_2, \quad (2)$$

where k_1, k_2 depend on the materials characteristics and θ_1, θ_2 are the angles between the wave travelling direction and the normal to the object surface. Usually the infrared wave is being transmitted and reflected through the same medium (the air, for instance), so $k_1 = k_2$ and, consequently, $\theta_1 = \theta_2$. Therefore, the desired distance between sensor and object can be obtained by measuring the intensities of the two waves.

However in most cases, it is hardly possible to know *a priori* the property of object material. To overcome this problem, one possible solution is to use the flight time, meaning that the sensor counts the time between the emission and reception of the infrared wave. The corresponding distance can be obtained as

$$d = \frac{vt_f}{2}, \quad (3)$$

where v is the wave propagation velocity, t_f is the flight time.

IV. GRASP REFINEMENT ALGORITHM

The IR sensors are mounted on the distal phalanges of a subset of the SoftHand fingers, according to the sensors' visibility of the object. Fig. 1 shows one of the possible arrangements of IR sensors, where only the thumb, index and ring finger are equipped. The sensor readings provide the distances between the phalanges and object within a range of ~ 60 mm. It is assumed that all sensor measurements are collected in a vector $\mathbf{d} = [d_1, d_2, \dots, d_n]^T$, $d_i \geq 0$, where n indicates the number of sensors whose measurement is available (i.e. the sensor is seeing the object). Corresponding residual errors can be simply written as $r_i = d_i$. Since the goal is for the hand to approach the object in a homogeneous manner, a reasonable choice for the cost function is the scaled squared norm of the residual vector, defined as follows

$$f = \frac{1}{2} \sum_{i=1}^n r_i^2 \quad (4)$$

This objective is in fact a function of control inputs via the dependence of the residual vector $\underline{\mathbf{r}} = [r_1, \dots, r_n]^T$ on control inputs $\underline{\mathbf{x}}$, which represent the decision variables of the optimization problem associated to hand centering. The size and nature of $\underline{\mathbf{x}}$ vary with the choice of the control inputs (e.g. for joint position control, $\underline{\mathbf{x}} = [j_1, \dots, j_n]^T$, for wrist pose control, $\underline{\mathbf{x}} = [p_x, \dots, p_z; r_x, \dots, r_z]^T$). In this case, $\underline{\mathbf{x}}$ is defined by the arm wrist pose $(p_x, p_y, p_z; r_x, r_y, r_z)$ (6 DoF) together with the amount of hand closing σ , which is directly the synergy actuation (1 DoF), therefore $\underline{\mathbf{x}} = [p_x, p_y, p_z; r_x, r_y, r_z; \sigma]^T$. The corresponding optimization problem can be formulated as

$$\min_{\underline{\mathbf{x}}} f(\underline{\mathbf{x}}), \quad \text{where } f(\underline{\mathbf{x}}) = \frac{1}{2} \underline{\mathbf{r}}(\underline{\mathbf{x}})^T \underline{\mathbf{r}}(\underline{\mathbf{x}}) \quad (5)$$

which is a *nonlinear* quadratic function w.r.t. the decision variables $\underline{\mathbf{x}}$.

It is worth noting that, in the experimental setting, $f(\underline{\mathbf{x}})$ is only computable through execution of moves and measurement of sensor outputs. To reconcile the use of a gradient-based optimization algorithm with the intrinsic numerical nature of our $f(\underline{\mathbf{x}})$, we employ a Gauss-Newton strategy and form a linear approximation of the residual as follows

$$\underline{\mathbf{r}}(\underline{\mathbf{x}}) \simeq \underline{\mathbf{r}}_L(\Delta \underline{\mathbf{x}}) = \underline{\mathbf{r}}(\underline{\mathbf{x}}_k) + \mathbf{J}_r(\underline{\mathbf{x}}_k) \cdot \Delta \underline{\mathbf{x}}, \quad \text{where } \mathbf{J}_r = \frac{\partial \underline{\mathbf{r}}}{\partial \underline{\mathbf{x}}} \quad (6)$$

such that the optimal solution can be found step by step via corrections of the control inputs such that $\underline{\mathbf{r}} \rightarrow 0$ as k increases. In (6), $\underline{\mathbf{r}}(\underline{\mathbf{x}}_k)$ is the residual measured at current step k , \mathbf{J}_r is the Jacobian matrix of the residuals, and $\Delta \underline{\mathbf{x}}$ is the displacement correction, which represents the next move. Here, \mathbf{J}_r is computed numerically based on the measurement data. In particular, each column can be approximated as

$$\mathbf{J}_r(:, j) \simeq \frac{\delta \underline{\mathbf{r}}}{\delta \underline{\mathbf{x}}_j} \quad (7)$$

where $\delta \underline{\mathbf{r}}$ collects the changes in the measurements of residuals vector with respect to the change in each control

input $\delta\mathbf{x}_j$. Using Eq. (5) and (6), one can obtain the solution of the quadratic approximation at k -th step

$$f_Q(\Delta\mathbf{x}_k) = \frac{1}{2}\mathbf{r}_L(\Delta\mathbf{x}_k)^T \mathbf{r}_L(\Delta\mathbf{x}_k) \quad (8)$$

of the original optimization problem (5) by seeking where $\frac{\partial f_Q(\Delta\mathbf{x}_k)}{\partial \Delta\mathbf{x}_k} = \mathbf{0}^T$, which yields

$$\Delta\mathbf{x}_k = -\mathbf{J}_r^+(\mathbf{x}_k) \mathbf{r}_k \quad (9)$$

Note that $\mathbf{J}_r^+ = (\mathbf{J}_r^T \mathbf{J}_r)^{-1} \mathbf{J}_r^T$ is the pseudo-inverse of the residual Jacobian. This allows us to update the subsequent hand location/configuration by adding the step as follows

$$\mathbf{x}_{k+1} = \mathbf{x}_k + \alpha \Delta\mathbf{x}_k \quad (10)$$

where $\alpha \in [0, 1]$ is proper scaling factor calibrated according to bounds on the robot and hand joint velocities.

Based on the above method for pre-grasp optimization, a detailed procedure is proposed which is summarized in Algorithm 1. It should be mentioned that the strategies for approaching and moving the end-effector in steps no. 4 and no. 5 seem ambiguous due to the fact that these strategies highly depends on the particular circumstance of the sensors arrangement and measurements. More details on this aspect will be provided in the Sec. V.

V. EXPERIMENTAL VALIDATION

To confirm the applicability of the proposed grasp refinement algorithm and to demonstrate its benefits from a practical perspective, this section presents the experimental setup and procedure, the sensor peculiarities, as well as the experimental results of in terms of grasping performances on a set of three everyday objects.

A. Experiment setup and procedure

To perform the grasping tasks, the following experimental setup was used:

- A RGB-D sensor, Asus Xtion ProLive [21], for acquisition of the object point cloud (frontal view only);
- A 7-DoF robotic manipulator, Kuka Lightweight IV [22], for object manipulation (maximum payload 7 kg);
- A 19-DoF, 1-DoA robotic hand, Pisa/IIT SoftHand, for object grasping;
- Three short-range IR sensors, Avago HDSL9100, mounted on three hand fingers (thumb, index and ring) for distance measurements;
- A table and a set of three selected everyday objects, including a cylinder, a baby cup and a paper box.

Assuming that the vision sensor captures the object frontal view only, the grasp experiments are meant to evaluate the performance of the infrared sensor-based pre-grasp optimization in two different scenarios: (\mathfrak{N}) nominal object pose: the object is in the nominal pose given by the vision sensor; (\mathfrak{P}) perturbed object pose: the object pose is different w.r.t. to the estimate provided by the vision sensor. In case (\mathfrak{N}), all objects are assumed to be grasped at their

Algorithm 1: Pre-Grasp Optimization

```

1: Acquiring object shape and location from a prior visual
cue and obtain a pre-grasp location for the robotic arm;

2: Moving the arm to the obtained location and bringing
the grasping end-effector to a pre-grasp configuration;

3: Checking the sensor measurements:
   if All sensors have no measurements on the object
   then
      Goto Step no. 4;
   if At least one sensor has measurement on the object
   then
      Goto Step no. 5;
   if All sensors have measurements on the object then
      Goto Step no. 6;
4: Approaching the grasping end-effector to the object
and returning to step no. 3;
5: Moving the grasping end-effector around the object
according to particular strategy (depending on the
sensors measurements), returning to step no. 3;
6: Moving the grasping end-effector by sequentially
changing each parameter of the control input  $\delta\mathbf{x}$ , while
obtaining the differences in residual vector  $\delta\mathbf{r}$  based on
sensor measurements and return the end-effector to its
previous state;
7: Computing the residual Jacobian matrix using Eq. (7);
8: Computing the corrections  $\Delta\mathbf{x}$  for the succeeding step
using Eq.(9);
9: Moving and closing the grasping end-effector following
Eq. (10), and reading the IR sensor measurements;
10: Computing the objective function  $f$  using the new
measurements:
   if  $f > \text{threshold}$  then
      Goto Step 6;
   else
      Goto Grasp the Object!

```

predefined positions on the table. For objects that do not possess any axis of symmetry, the grasping experiments are performed with the object in two different orientations. For each object and each orientation, experiments are repeated three times. In case (\mathfrak{P}), the same protocol of case (\mathfrak{N}) is repeated, except that objects are slightly moved away from their nominal positions (in translations and/or in orientation, depending on the symmetrical properties of corresponding object). Details relate to object poses are illustrated in Fig. 5. For comparison, grasping experiments are carried out both with and without applying the IR sensor-based optimization algorithm proposed. To demonstrate the advantages of our method, the analysis of grasping performances is presented in the following subsections, in terms of successful grasp rate. Then, the evolution of measured distances is presented to evaluate the converge behavior of the underlying optimization process.

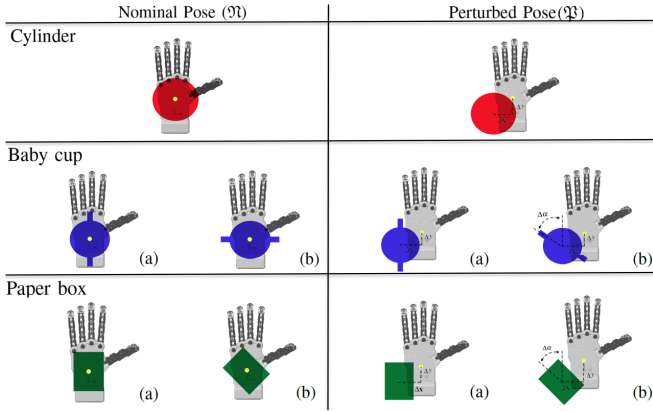


Fig. 5. Nominal (\mathfrak{N}) and Perturbed (\mathfrak{P}) object poses in grasping experiments

B. Sensor features and measured outputs

In this work, the Avago HDSL9100 Infrared Sensor [23] (see Fig. 6) is selected due to its small size (7x3x2.5 mm), which fits the fingertips of Pisa/IIT SoftHand and provides a suitable operative range (4-65 mm) for the distance measurements. However, due to the small size of the sensor, a conditioning circuit is required to properly scale the sensor inputs and outputs. It goes without saying that the sensor operative range depends on the circuit components: here, they are tuned to obtain the maximum distance.

Another issue is related to the reciprocal position of the sensors on the fingerpads of the SoftHand. In our experiment, three IR sensors are used which are mounted on the thumb, index and ring fingers (see Fig. 1). This arrangement may cause some disturbances during the measurements: for instance, the light emitted by one sensor could be misread by another one. To overcome this problem, the conditioning circuit is designed to activate only one sensor at a time in a cyclic fashion.

The schematic of the conditioning circuit is illustrated in Fig. 7, where each sensor is activated by a square wave (D_o), and its output is read by an analog-digital converter (ADC). The physical output of the sensor is an electric voltage, which is proportional to the intensity of the reflected wave acquired by the receiver. Therefore, the higher the output voltage, the closer is the sensor to the object. The ADC returns the output voltage in a digital value in bits (or ticks), according to its resolution (12 bits on 5 Volt for the embedded microcontroller PSoC).

To simplify the design of conditioning circuit, instead

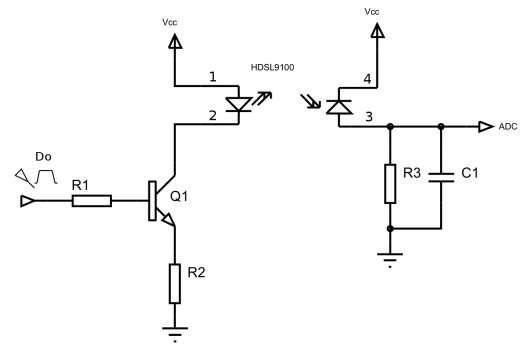


Fig. 7. Conditioning circuit schematic of IR sensor

of counting the sensor flight time (see Section III), which would need a dedicated electronic stage, we used directly the output value of the ADC. However, since the proposed algorithm, step by step along the local gradient, aims to reduce the mean squared distance between the object and the robot end-effector, it needs a measure of distance to operate properly. It moves the end-effector of the robot and concurrently measures the distances, to understand which movements allows for a reduction in the overall distance.

Therefore, an exact measure of distance would be ideally needed. However, this would call for a calibration procedure that might change from object to object due to different reflective properties of the material.

Interestingly enough, we found that in order to give satisfactory results, the algorithm does not need the exact value of distances, but a relative estimate with respect to the initial measure is enough.

The constant calibration curve that we employed in all the experiments is depicted in Fig. 8 and was obtained by approximating the experimental data with the following model

$$y = ae^{bx} + ce^{dx}, \quad (11)$$

which maps the ADC output x to the desired distance y . The estimated parameters a, b, c, d vary only slightly from one sensor to another due to the tolerances of conditioning circuit components.

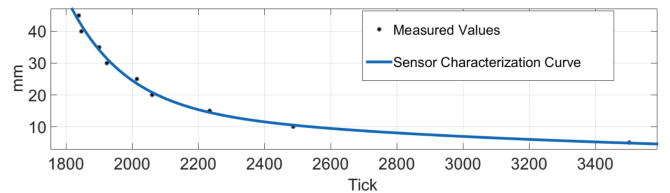


Fig. 8. Characterization curve of one IR Sensor

C. Sensor measurements checks

According to Algorithm (1), at Step no. 3, one has to ensure that all sensors are in their operative ranges. To this end, we proposed an heuristic strategy to steer the SoftHand in a way that all sensors come to see the object and the pre-grasp optimization procedure can be started. Fig. 9 illustrates

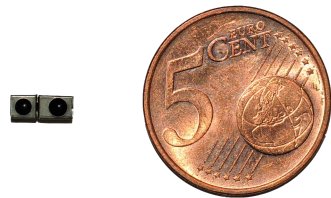


Fig. 6. Avago HDSL9100 Infrared Sensors

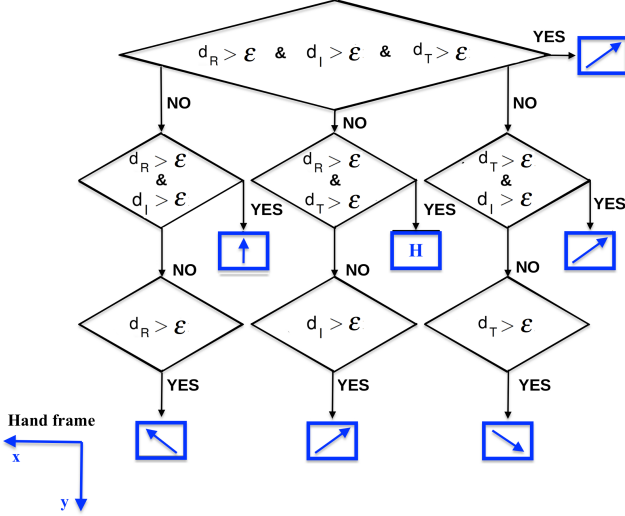


Fig. 9. All possible cases of sensor visibilities (ϵ is set to the maximum operative range 60mm)

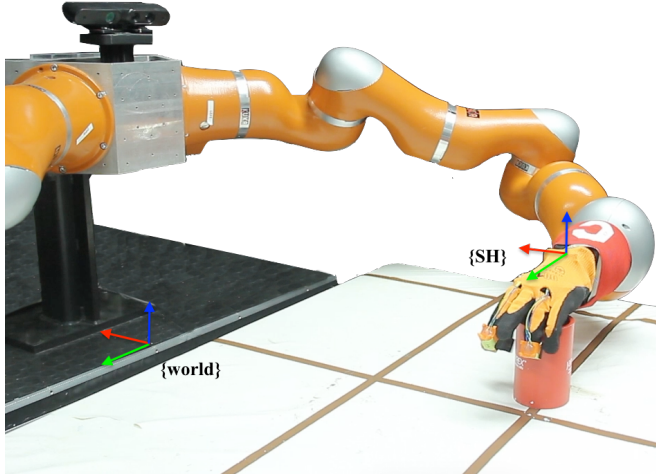


Fig. 10. The SoftHand frame $\{SH\}$ and world frame $\{world\}$

all the possible situations where one or more sensors lose the object and the corresponding recovering actions that should be executed by the hand. In total, there are seven different cases and five possible actions to perform. Four of the actions (indicated with blue arrows) represent linear motions the hand should perform. The remaining action (indicated with H) represents hand closing. The displacement indicated by the arrows should be interpreted in the world frame (see lower left reference frame in Fig. 9 and also Fig. 10).

D. Grasp results

The results of the grasping experiments are given in Table I, where the number of successful grasps are provided for each object. Comparison are made for grasping with and without the proposed algorithm, which are labelled as IR-guided and Blind, respectively.

This table shows the number successful grasps with respect to the trials performed. Each row refers to an object in

Object and reference pose	Nominal Pose (\mathfrak{N})		Perturbed Pose (\mathfrak{P})	
	IR-guided	Blind	IR-guided	Blind
Cylinder	2/3	0/3	3/3	0/3
Baby cup, pose (a)	1/3	0/3	1/3	0/3
Baby cup, pose (b)	3/3	1/3	2/3	0/3
Paper box, pose (a)	3/3	0/3	1/3	0/3
Paper box, pose (b)	2/3	1/3	1/3	0/3
Total	11/15	2/15	8/15	0/15

TABLE I
SUCCESSFUL GRASPS FOR DIFFERENT OBJECTS IN NOMINAL (\mathfrak{N}) AND PERTURBED (\mathfrak{P}) POSE, WHEN EMPLOYING IR-GUIDED OR BLIND GRASP STRATEGIES.

Object	Nominal Pose (\mathfrak{N})			Perturbed Pose (\mathfrak{P})		
	Index	Thumb	Ring	Index	Thumb	Ring
Cylinder	0.033	0.009	0.012	0.057	0.017	0.018
Baby cup	0.030	0.010	0.012	0.048	0.018	0.019
Paper box	0.033	0.011	0.010	0.029	0.015	0.013

TABLE II
DISTANCE MEASUREMENTS OF DIFFERENT HAND FINGERTIPS IN NOMINAL AND PERTURBED POSE, AT THE LAST STEP OF IR-GUIDED GRASP PLAN [M]

a reference pose. The first two columns report the successful grasps in the nominal (\mathfrak{N}) object pose, for IR-guided and Blind grasps, respectively. The third and fourth columns report the successful grasps in the perturbed (\mathfrak{P}) object pose, for IR-guided and Blind grasps, respectively.

Clearly, using only the prior visual cue of the object and performing the grasp task at corresponding nominal pre-grasp location, the number of successful grasps is very low, even in the nominal case (\mathfrak{N}). In the case of perturbed grasp (\mathfrak{P}), i.e. when the object is deliberately moved, the successful grasps drop to zero, as the perturbation is sufficient for the hand to completely miss the object. Applying the proposed sensor-based grasp planner, the successful rate considerably increases from 13% to 73% in case (\mathfrak{N}), and from 0% to 53% in case (\mathfrak{P}), respectively. Fig. 11 shows two time sequences of the IR-guided strategy when grasping the baby cup in configuration (a), nominal pose (\mathfrak{N}) (see Fig. 5, first column) and in configuration (a), perturbed pose (\mathfrak{P}) (see Fig. 5, second column). A video of the IR-guided grasping strategy can be found at the following [youtube channel](#).

Fig. 12 shows plots of the sensor measurements during the execution of some of the IR-guided grasp experiments performed in the nominal case (\mathfrak{N}). Here, the convergence behavior of the optimization algorithm can be evaluated. In particular, the red line describes the evolution of the Euclidean norm of the residual, i.e. the cost function being minimized. The other three curves show separately the distance measured from the index, thumb and ring fingertips to the object at each time step. Fig. 13 illustrates the same quantities when grasping in perturbed poses (\mathfrak{P}).

It is worth noting that the cost function employed in the documented experiments considered only the contributions associated to the thumb and the ring fingers. The reason for this choice was motivated by the fact that due to Softhand

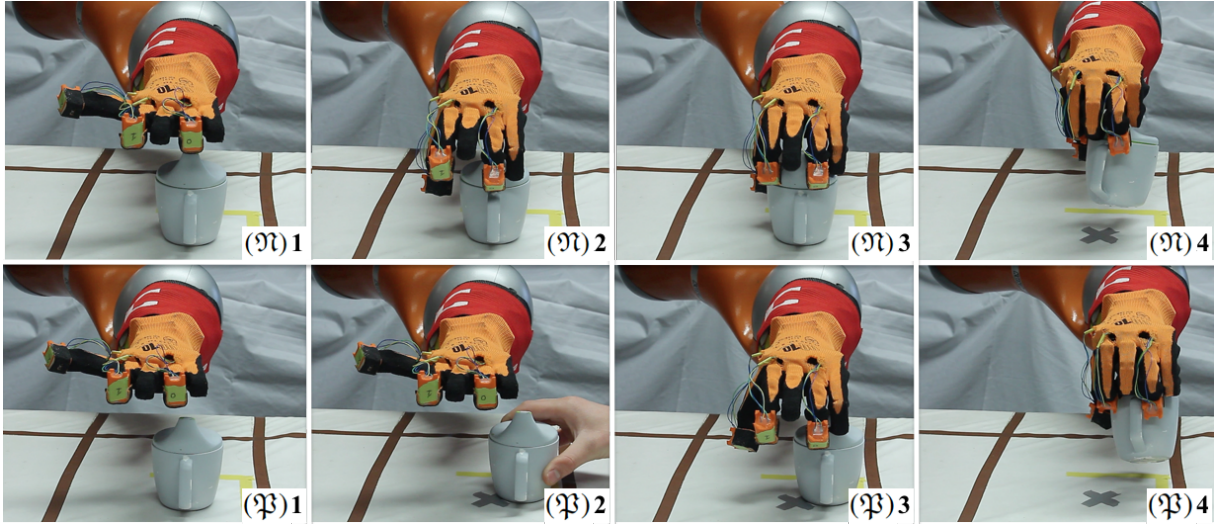


Fig. 11. Snapshots of the IR-guided grasp of the baby cup. First row: baby cup in configuration (a), nominal pose (\mathfrak{M}) (see Fig. 5, first column). Second row: baby cup in configuration (a), perturbed pose (\mathfrak{M}) (see Fig. 5, second column).

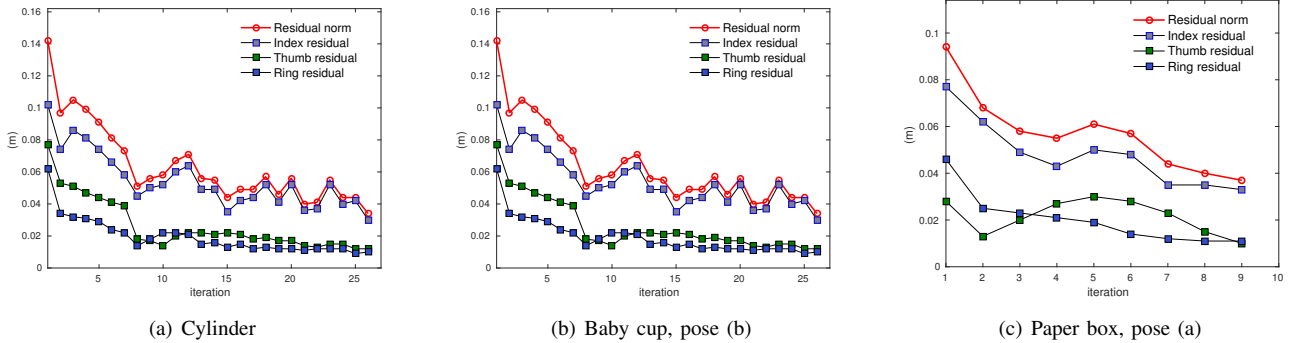


Fig. 12. Sensor measurements during execution of grasps in nominal object pose (\mathfrak{M})

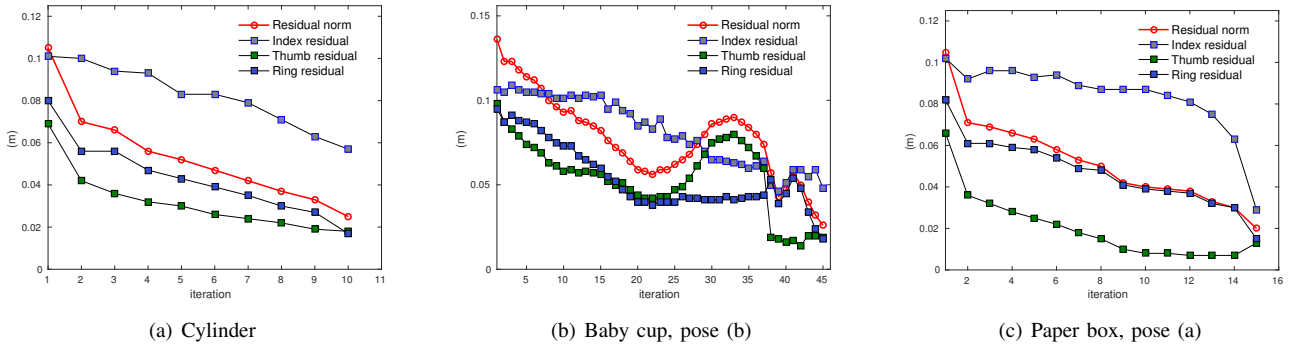


Fig. 13. Sensor measurements during execution of grasps in perturbed object pose (\mathfrak{M})

closing pattern, the index finger lagged behind, while the others were close to contacting with the object.

From Figs. 12 and 13, it is clear that the proposed sensor-informed grasp planner succeeds in reducing the distances from the SoftHand fingertips to the object, paving the way to a successful open-loop grasp from that point on, in accordance to the successful grasp rate reported in Table I. Finally, it is worth noting that, in most of the performed grasping

tasks, a success has been registered when closing open-loop the hand from a distance of three to four centimeters to the object.

Table II presents more in details the measured distances between different hand fingertips and objects, when the IR-guided grasp planner was applied. In most of the performed grasping tasks, results confirm that the index fingertips is always further from the object than the other two fingers,

whereas the thumb and ring are well centered with respect to the object. This is due to the synergy mechanically encoded in the SoftHand: each finger closes differently even if the actuation cable is pulled with the same force. This behavior of the SoftHand has to be further investigated as a future work if such a centering strategy has to be extended to multiple fingers and, possibly, multiple phalanges per finger.

VI. CONCLUSIONS

In this paper we have presented an effective and efficient method to refine the final grasping pose of a soft robotic hand with respect an object, using low-cost IR sensors. The problem has been framed as a nonlinear optimization one, where the mean distance between the sensorized fingerpads and the object is minimized. An algorithm has been proposed which allows to apply Gauss-Newton steps to command the hand pose with the goal of centering the hand around an object, whose location and shape have been acquired through vision and can be altered significantly. The algorithm was tested on a Kuka-LWR arm and a Pisa/IIT Softhand by performing grasp tasks in the presence of uncertainty in the object pose. The outcomes showed the effectiveness of the proposed method and essential improvement in the grasping performance with respect to a blind grasping strategy. Future work will address the full use of the IR sensors on all fingers, taking into account the adaptive synergy of the softhand, to exploit the capabilities of the sensorized Softhand for perceiving unstructured environments.

VII. ACKNOWLEDGMENTS

This work is supported by the grant no. 600918 PAC-MAN - Probabilistic and Compositional Representations of Object for Robotic Manipulation - within the FP7-ICT-2011-9, and under grant agreement no. 645599 SoMa - Soft-bodied intelligence for Manipulation, within the H2020-ICT-2014-1.

REFERENCES

- [1] A. Bicchi and V. Kumar, "Robotic grasping and contact: a review," in *Robotics and Automation, 2000. Proceedings. ICRA '00. IEEE International Conference on*, vol. 1, 2000, pp. 348–353.
- [2] A. M. Okamura, N. Smaby, and M. R. Cutkosky, "An overview of dexterous manipulation," in *Robotics and Automation, 2000. Proceedings. ICRA'00. IEEE International Conference on*, vol. 1. IEEE, 2000, pp. 255–262.
- [3] C. C. Kemp, A. Edsinger, and E. Torres-Jara, "Challenges for robot manipulation in human environments," *IEEE Robotics and Automation Magazine*, vol. 14, no. 1, p. 20, 2007.
- [4] R. Diankov and J. Kuffner, "Openrave: A planning architecture for autonomous robotics," *Robotics Institute, Pittsburgh, PA, Tech. Rep. CMU-RI-TR-08-34*, vol. 79, 2008.
- [5] A. Miller and P. Allen, "Graspit! a versatile simulator for robotic grasping," *Robotics Automation Magazine, IEEE*, vol. 11, no. 4, pp. 110–122, 2004.
- [6] C. Kemp, C. Anderson, H. Nguyen, A. Trevor, and Z. Xu, "A point-and-click interface for the real world: Laser designation of objects for mobile manipulation," in *Human-Robot Interaction (HRI), 2008 3rd ACM/IEEE International Conference on*, Mar. 2008, pp. 241–248.
- [7] A. Saxena, J. Driemeyer, and A. Y. Ng, "Robotic grasping of novel objects using vision," *The International Journal of Robotics Research*, vol. 27, no. 2, pp. 157–173, 2008.
- [8] B. Wang, L. Jiang, J. Li, and H. Cai, "Grasping unknown objects based on 3d model reconstruction," in *Advanced Intelligent Mechatronics. Proceedings, 2005 IEEE/ASME International Conference on*, Jul. 2005, pp. 461–466.
- [9] J. Tegin and J. Wikander, "Tactile sensing in intelligent robotic manipulation-a review," *Industrial Robot: An International Journal*, vol. 32, no. 1, pp. 64–70, 2005.
- [10] L. Natale and E. Torres-Jara, "A sensitive approach to grasping," in *Proceedings of the sixth international workshop on epigenetic robotics*. Citeseer, 2006, pp. 87–94.
- [11] J. Romano, K. Hsiao, G. Niemeyer, S. Chitta, and K. Kuchenbecker, "Human-inspired robotic grasp control with tactile sensing," *Robotics, IEEE Transactions on*, vol. 27, no. 6, pp. 1067–1079, Dec. 2011.
- [12] L. U. Odhner, L. P. Jentoft, M. R. Claffee, N. Corson, Y. Tenzer, R. R. Ma, M. Buehler, R. Kohout, R. D. Howe, and A. M. Dollar, "A compliant, underactuated hand for robust manipulation," *The International Journal of Robotics Research*, vol. 33, no. 5, pp. 736–752, 2014.
- [13] R. Deimel and O. Brock, "A novel type of compliant and underactuated robotic hand for dexterous grasping," *The International Journal of Robotics Research*, p. 0278364915592961, 2015.
- [14] M. G. Catalano, G. Grioli, E. Farnioli, A. Serio, C. Piazza, and A. Bicchi, "Adaptive synergies for the design and control of the pisa/iit softhand," *The International Journal of Robotics Research*, vol. 33, no. 5, pp. 768–782, 2014.
- [15] M. Bonilla, E. Farnioli, C. Piazza, M. Catalano, G. Grioli, M. Garabini, M. Gabiccini, and A. Bicchi, "Grasping with soft hands," in *Humanoid Robots (Humanoids), 2014 14th IEEE-RAS International Conference on*. IEEE, 2014, pp. 581–587.
- [16] D. Gunji, Y. Mizoguchi, S. Teshigawara, A. Ming, A. Namiki, M. Ishikawa and, and M. Shimojo, "Grasping force control of multi-fingered robot hand based on slip detection using tactile sensor," in *Robotics and Automation, 2008. ICRA 2008. IEEE International Conference on*, May 2008, pp. 2605–2610.
- [17] J. Felip and A. Morales, "Robust sensor-based grasp primitive for a three-finger robot hand," in *Intelligent Robots and Systems, 2009. IROS 2009. IEEE/RSJ International Conference on*. IEEE, 2009, pp. 1811–1816.
- [18] K. Hsiao, P. Nangeroni, M. Huber, A. Saxena, and A. Ng, "Reactive grasping using optical proximity sensors," in *Robotics and Automation, 2009. ICRA '09. IEEE International Conference on*, May 2009, pp. 2098–2105.
- [19] N. Chen, K. P. Tee, and C.-M. Chew, "Teleoperation grasp assistance using infra-red sensor array," *Robotica*, vol. 33, no. 04, pp. 986–1002, 2015.
- [20] S. Ye, K. Suzuki, Y. Suzuki, M. Ishikawa, and M. Shimojo, "Robust robotic grasping using IR net-structure proximity sensor to handle objects with unknown position and attitude," in *Robotics and Automation (ICRA), 2013 IEEE International Conference on*, May 2013, pp. 3271–3278.
- [21] "Asus xtion pro live home page," online; accessed 22-February-2016. [Online]. Available: https://www.asus.com/3D-Sensor/Xtion_PRO_LIVE/
- [22] R. Bischoff, J. Kurth, G. Schreiber, R. Koeppe, A. Albu-Schaffer, A. Beyer, O. Eiberger, S. Haddadin, A. Stemmer, G. Grunwald, and G. Hirzinger, "The kuka-dlr lightweight robot arm - a new reference platform for robotics research and manufacturing," in *Robotics (ISR), 2010 41st International Symposium on and 2010 6th German Conference on Robotics (ROBOTIK)*. IEEE, 2010.
- [23] "HdsI9100 datasheet page," online; accessed 18-February-2016. [Online]. Available: <http://www.avagotech.com/docs/AV02-2259EN>